A Sea-Surface Radiation Data Set for Climate Applications in the Tropical Western Pacific and South China Sea

Ming-Dah Chou, Pui-King Chan[1], and Michael M.-H. Yan[2]
Laboratory for Atmospheres
NASA/Goddard Space Flight Center
Greenbelt, MD 20771

April, 2000
To be submitted to Journal of Geophysical Research

1. Universities Space Research Association, Seabrook, MD 20706
2. Science Systems and Applications, Inc., Lanham, MD 20706.

Abstract

The sea-surface shortwave and longwave radiative fluxes have been retrieved from the radiances measured by Japan's Geostationary Meteorological Satellite 5. The surface radiation data set covers the domain 40°S-40°N and 90°E-170°W. The temporal resolution is 1 day, and the spatial resolution is 0.5°x0.5° latitude-longitude. The retrieved surface radiation have been validated with the radiometric measurements at the Atmospheric Radiation Measuring (ARM) site on Manus island in the equatorial western Pacific for a period of 15 months. It has also been validated with the measurements at the radiation site on Dungsha island in the South China Sea during the South China Sea Monsoon Experiment (SCSMEX) Intensive Observing Period (May and June 1998). The data set is used to study the effect of El Nino and East Asian Summer monsoon on the heating of the ocean in the tropical western Pacific and the South China Sea. Interannual variations of clouds associated with El Nino and the East Asian Summer monsoon have a large impact on the radiative heating of the ocean. It has been found that the magnitude of the interannual variation of the seasonal mean surface radiative heating exceeds 40 W m^{-2} over large areas. Together with the Clouds and the Earth's Radiant Energy System (CERES) shortwave fluxes at top of the atmosphere and the radiative transfer calculations of clear-sky fluxes, this surface radiation data set is also used to study the impact of clouds on the solar heating of the atmosphere. It is found that clouds enhance the atmospheric solar heating by ~20 W m^{-2} in the tropical western Pacific and the South China Sea. This result is important for evaluating the accuracy of solar flux calculations in clear and cloudy atmospheres.

1. Introduction

Over tropical oceans, approximately 20% of the incoming solar radiation at the top of the atmosphere is reflected by the ocean-atmosphere system, 25% is absorbed in the atmosphere, and 55% is absorbed by the ocean. Surface radiation over the ocean is an essential component of the Earth's radiation budgets in atmospheric and oceanic studies. The information on surface radiation is important for understanding the processes that affect the sea surface temperature (e.g. *Chou et al.*, 2000). It can also serve as a boundary condition for model simulations of oceanic general circulation.

The Global Energy Balance Archive (GEBA) project compiles global surface radiation budget with high quality control [*Gilgen and Ohmura*, 1999]. The GEBA data set has been widely used for climate studies, including validations of the satellite remote sensing and climate model simulation, and impacts of clouds and aerosols on atmospheric and surface heating, This very useful data set comprises surface radiometric SW and LW flux measurements mostly over continents. Data over oceanic regions are scarce. Another source of the surface radiation budget data is the eight-year Surface Radiation Budget data set developed at NASA Langley Research Center [*Gupta et al.*, 1999]. It is derived from the ISCCP radiances [*Rossow and Schiffer*, 1991]. This data set has a global coverage and a spatial resolution of ~2.5°x2.5° latitude-longitude. It is being expanded to cover more years with a spatial resolution of 1°x1° latitude-longitude

Starting from January 1998, we have been receiving Japan's Geostationary Meteorological Satellite 5 (GMS-5) radiances at NASA Goddard Space Flight Center on daily basis. We have derived the surface downward solar (shortwave, or SW) and thermal infrared (longwave, or LW) fluxes from the GMS-measured albedo in the visible spectral channel and the brightness temperature in the thermal infrared window. This surface radiation data set covers the region 40°S-40°N, 90°E-170°W. It has a temporal resolution of 1 day and a spatial resolution of 0.5°x0.5° latitude-longitude. In addition to oceanic and atmospheric studies, this data set can also be used for intercomparison with other surface radiation data sets.

We use this surface radiation data set to investigate the effect of El Nino on the surface radiation budget in the tropical western Pacific (TWP) and the South China Sea (SCS). Combined with the SW flux at the top of the atmosphere (TOA) derived from the

Tropical Rain Measuring Mission (TRMM) Clouds and the Earth's Radiant Energy System (CERES) measurements [*Wielicki, et al.*, 1996], this data set is also used to investigate the effect of clouds on the solar heating of the atmosphere, or atmospheric cloud radiative forcing (CRF). The sources of data used in this study are given in Section 2. Section 3 presents satellite retrieval algorithms for deriving the surface radiation in the TWP and validation of the satellite-retrieved surface radiation against radiometric measurements. Section 4 investigates the temporal and spatial distributions of the TWP surface radiation budgets. Application of the data set to study the effect of clouds on the atmospheric solar heating is given in Section 5. A summary is given in Section 6.

2. Data Sources

All-sky surface radiation is derived from the radiances measured by Japan's Geostationary Meteorological Satellite 5 (GMS-5). The satellite is positioned above the Equator and 140° E longitude. It measures the Earth's emitted and reflected radiances at 4 narrow spectral channels. The temporal resolution is 1 hr and the spatial resolution is 5 km at the subsatellite point. Because of the curvature of the Earth, the usefulness of the data is limited to the region within 50° (latitude and longitude) of the subsatellite point. At NASA Goddard Space Flight Center, we have been receiving the raw data on daily basis since January 1998.

The all-sky surface downward SW flux is derived as a function the albedo in the 0.7-μm channel (α_v) and the solar zenith angle. The albedo is measured by the GMS-5, and the solar zenith angle is computed from the latitude, longitude, date of the year, and local time. The all-sky surface downward LW flux is derived as a function of the brightness temperature (T_b), the column water vapor amount (w), and the sea surface temperature (SST, or T_s). The brightness temperature is measured by the GMS-5 in the 11-μm infrared window channel. The column water vapor amount is taken from *Wentz* [1994]. He derived the column water vapor amount using the radiances measured by the Special Sensor Microwave/Imager (SSMI) on board of the Defense Meteorological Satellite Program (DMSP) satellites. The water vapor data have a temporal resolution of 1 day and a spatial resolution of 2.0°x2.5° latitude-longitude. The SST data are taken from the National Centers for Environmental Prediction (NCEP). The SST was derived

empirical from the satellite-measured radiances in infrared window channels [*Reynolsd and Smith*, 1994]. It has a temporal resolution of 1 week and a spatial resolution of 1°x1° latitude-longitude. In this study, the water vapor amount is interpolated to a spatial resolution of 1°x1° latitude-longitude, and the SST is interpolated to a temporal resolution of 1 day.

The clear-sky surface SW radiation used to estimate the atmospheric CRF is computed using a radiation parameterization developed for cloud and climate model studies [*Chou and Suarez*, 1999]. It includes the absorption due to water vapor, O_3, O_2, and CO_2, clouds, and aerosols. Interactions among the absorption and scattering by clouds, aerosols, molecules (Rayleigh scattering), and the surface are fully taken into account. Fluxes are integrated virtually over the entire spectrum from 0.175 μm to 10μm.

The surface radiation data set is validated with the measurements at Dungsha island (20.70°N, 116.72°E) in the SCS and at the Atmospheric Radiation Measurement (ARM) site on Manus island (2.06°S, 147.43°E) in the TWP. The clear- and all-sky SW fluxes at the TOA used for estimating the atmospheric CRF (Section 5) are taken from TRMM CERES archive. The CERES ES-4 data have the same format as the Earth Radiation Budget Experiment (ERBE) S-4. The temporal resolution is 1 month and the spatial resolution is 2.5°x2.5° latitude-longitude. Currently, data are available only for the period January-August 1998.

3. Derivation and Validation of Surface Radiation

3.1. Satellite Retrieval

The surface radiation budgets can be either computed using radiative transfer models [e.g. *Chou*, 1994; *Zhang et al.*, 1995] or derived from satellite radiance measurements using empirical correlation between the surface flux measurements and the satellite radiance measurements [e.g. *Li and Leighton*, 1993; *Pinker et al.*, 1995]. The former approach explicitly takes into account the physical processes of radiative transfer. Because surface radiation is sensitive to clouds and because the satellite-retrieval of cloud optical properties and macro-physical structure (three dimensional configuration and fractional cover) is expected to have a large uncertainty, radiative transfer calculations are also subject to a large uncertainty. On the other hand, the surface SW flux is highly

correlated with the radiation at the TOA, whereas the surface LW flux is only weakly correlated with the radiation at the TOA.

For the reasons mentioned above, *Chou et al.* [1998] used the second approach to empirically derive the surface SW and LW fluxes from the radiances measured by Japan's GMS-4 satellite. The radiance measurements had a spatial resolution of 5 km and a temporal resolution of 1 hour. The surface downward SW flux, $S_s^{\downarrow}$, was related to the GMS-measured albedo, α_v, in the visible spectral region centered at 0.7 μm,

$$S_s^{\downarrow} = Q_o \mu_o \tau(\alpha_v, \mu_o) \tag{1}$$

where μ_o is the cosine of the solar zenith angle, $Q_o\mu_o$ is the incoming solar radiation at the TOA, τ is the mean atmospheric transmittance of the entire solar spectrum. Based on the GMS-4 albedo measurements and the surface radiation measurements during the Tropical Ocean Global Atmosphere (TOGA) Coupled Ocean-Atmosphere Response Experiment (COARE) Intensive Observing Period (November 1992-February 1993), a table for the transmission function τ was derived and used to compute surface SW flux over the entire Pacific warm pool.

Except in the 10-μm spectral window region, the lower troposphere in the tropics is quite opaque. The surface downward LW radiation is primarily determined by the temperature and humidity of the atmospheric boundary layer. Clouds also have a large effect on the surface LW radiation primarily in the 11-μm window region, which can be related to the satellite radiance measurements in the IR window channel. Based on the surface flux measurements and satellite radiance measurements during the TOGA COARE IOP, *Chou et al.* [1998] derived the downward LW flux using the following empirical function,

$$F_s^{\downarrow} = (502-0.464\, T_b-6.75w+0.0565wT_b)\,(T_s/T_o)^4 \tag{2}$$

where w is the column water vapor amount, T_b is the GMS-measured brightness temperature in the 11-μm window channel, T_s is the sea surface temperature, and T_o=293K. Units are g cm^{-2} for w and K for T_b and T_s. Equation (2) shows that the surface downward LW flux is most sensitive to lower tropospheric humidity and only weakly

related to the radiation at the top of the atmosphere. The lower tropospheric temperature is highly correlated with the sea surface temperature. Its effect on the surface downward LW flux is taken into account through the effect of T_s given in Equation (2).

The transmission table in Equation (1) and the regression coefficients in Equation (2) were derived based on the surface SW and LW fluxes measured at 6 sites on islands, research ships, and a buoy during the TOGA COARE IOP.

3.2. Validations

Chou et al. [1998] showed that the surface SW and LW fluxes derived from Equations (1) and (2) using the radiances measured by GMS-4 during the COARE IOP agreed very well with the surface measurements at seven surface radiation sites on small islands, onboard research ships, and on a buoy. Equations (1) and (2) were derived for the albedo in the visible spectral region and the brightness temperature in the IR window region measured by GMS-4. Since calibrations of radiances measured by different satellites are not necessarily the same, regressions such as Equations (1) and (2) derived from data measured by a satellite may not be applicable to other satellite data. Especially when there are no in-flight calibrations of the radiances measured by GMS-4 and 5. It requires justifications when applying Equations (1) and (2) to α_v and T_s measured by GMS-5.

The Atmospheric Radiation Measurement (ARM) program of the US Department of Energy established an Atmospheric Radiation and Cloud Station (ARCS) in the TWP to measure and study clouds, radiation, and atmospheric properties [*Mather et al.*, 1998]. This site is located on the island of Manus (2.06°S, 147.43°E), 300 km north of New Guinea. It began operation in October 1996 and plans to continue for 10 years. Among the comprehensive suite of instruments are the pyranometers for measuring broadband SW (0.3-4μm) fluxes and the pyrgeometers for measuring broadband LW (5-50 μm) fluxes. The surface radiative fluxes have a temporal resolution of 1 min. They are averaged to a resolution of 1 day for comparing with the GMS-derived fluxes. The latest ARM ARCS data available to this study is March 1998. Therefore, the comparison is only for the 15-month period from January 1998 to March 1999.

The original GMS-retrieved surface SW and LW fluxes have a spatial resolution of 0.5°x0.5° latitude-longitude and a temporal resolution of 1 hr. They are subsequently averaged to daily-mean values. Since the Manus ARCS site is located nearly at a corner of a 0.5°x0.5° latitude-longitude region, the GMS-retrieved fluxes of four neighboring grid boxes (1.5°S-2.5°S; 147°E-148°E) are averaged for comparing with the Manus measurements.

Figure 1 shows the daily variation of the downward SW fluxes, $S_s^{\downarrow}$, measured at the Manus ARCS site (solid curve) and retrieved from α_v measured by GMS-5 (dashed curve). The time series covers a total of 15 months from January 1998 to March 1999. Each point represents the daily-mean flux. Because of some missing GMS data, neighboring points are not necessarily consecutive days. Generally, the two curves follow each other very well. It is interesting that on certain days, $S_s^{\downarrow}$ is extremely small (<50 W m^{-2}), indicating heavy cloudiness throughout daytime hours. Figure 2 shows the scatter plot of the measured and retrieved $S_s^{\downarrow}$. It is the same as Figure 1, except presented in a different form. Averaged over the entire 15-month period, $S_s^{\downarrow}$ is 224 W m^{-2} from surface measurements and 231 W m^{-2} from satellite retrievals. The bias is 7 W m^{-2}. The rms difference of the daily $S_s^{\downarrow}$ is 30.3 W m^{-2}. This agreement is very good in view of the spatial inconsistency between satellite and surface measurements, as well as the potential error in surface radiometric measurements.

Figure 3 shows the daily variation of the downward LW fluxes, $F_s^{\downarrow}$, measured at the Manus ARCS site (solid curve) and retrieved from T_s measured by GMS-5 (dashed curve). It covers a period of 15 months from January 1998 to March 1999. Because of some missing GMS data, neighboring points are not necessarily consecutive days. The range of daily variation is small, ~400-440 W m^{-2}. This is a well acknowledged situation in the tropics, arising from a rather opaque (in the infrared) atmospheric boundary layer. The agreement between the measured and retrieved $F_s^{\downarrow}$ is very good. Averaged over the 15 months, $F_s^{\downarrow}$ is 424 W m^{-2} from surface measurements and 425 W m^{-2} from satellite retrievals. The rms difference of the daily $F_s^{\downarrow}$ is only 6.6 W m^{-2}.

An intensive filed campaign of the South China Sea Monsoon Experiment was conducted during May and June 1998. The SCSMEX is an international field experiment for studying the physical processes and evolutions of the water and energy cycles of the Southeast Asian monsoon system [*Lau et al.*, 2000]. A suite of instruments was set up at the small coral island of Dungsha (20.70°N, 116.72°E) to measure surface radiation and atmospheric temperature, humidity, and aerosols. Three Epply Precision Spectral Pyranometers (PSP) and one Yankee Total Spectral Pyranometer were used to measure and intercompare surface SW fluxes. The Epply pyranometers used specific band-passed Schott glass filters to measure fluxes in the ultraviolet (UV, 0.3~0.4 μm), photosynthetically active radiation (PAR, 0.4~0.7 μm), and infrared (IR, 0.7~2.8 μm) spectral bands. The total-band surface downward LW fluxes were measured using two Epply Precision Infrared Radiometers for intercomparison. A single data-acquiring system processed and stored all radiation measurements with a one-minute sampling rate.

Figure 4 shows daily variations of $S_s^{\downarrow}$ measured at Dungsha (solid curve) and retrieved from GMS-measured albedo (dashed). Since Dungsha is located near a corner of a 0.5°x0.5° latitude-longitude grid, the satellite-retrieved $S_s^{\downarrow}$ shown in the figure is the mean values of a 1°x1° latitude-longitude region with Dungsha located near the center. Because of missing data, there are only 35 (out of 50) daily values given in the figure. Neighboring points are not necessarily consecutive days. The two sets of data follow each other very well. Figure 5 is the scattering plot showing the same data as in Figure 4. Averaged over the 35 days, $S_s^{\downarrow}$ is 211 W m^{-2} from surface measurements and 214 W m^{-2} from satellite retrievals. The rms difference of the daily SW fluxes is only 17 W m^{-2}. Comparisons are not made for $F_s^{\downarrow}$ due to problems encountered in the data logging of LW flux measurements at Dungsha.

To reduce the bias between the surface measurements and satellite retrieval of $S_s^{\downarrow}$, the albedo measured by the GMS-5 is empirically adjusted by a factor β,

$$\alpha_v' = \beta\, \alpha_v \tag{3}$$

It is found that the bias is eliminated for β =1.013. It is likely that over long period of time, there is "drifting" of the satellite measurements. In such a situation, the factor β should also change with time. With well-controlled surface radiation measurements, Information on the variation of β with time can serve as an indicator for the "drifting" of satellite measurements. In principle, an approach similar to Equation (3) can be applied to T_b. . Since the bias of $F_s^{\downarrow}$ is small, no attempt has been made to adjust T_b.

4. Spatial and Interannual Variation

All-sky sea-surface SW and LW fluxes have been derived for a period of 20 months from January 1998 to August 1999. The albedo measured by GMS-5 is first adjusted according to Equation (3). The adjusted albedo, α_v, and the brightness temperature, T_b, are then averaged to 0.5°x0.5° latitude-longitude grids, and hourly surface fluxes are derived using Equations (1) and (2). Subsequently, the hourly data are averaged to daily values. The column water vapor amount, *w*, used in Equation (2) is taken from the SSMI retrieval by *Wentz*, [1994], and the sea surface temperature, T_s, is taken from the NCEP data archive [*Reynolds and Smith*, 1994]. The SSMI column water vapor amount represents daily-mean values, and the NCEP sea surface temperature represents weekly-mean values. They are taken as hourly values within either a day for *w* or a week for T_s. Both *w* and T_s have a spatial resolution of 1°x1° latitude-longitude. They are assumed to be constants for the four 0.5°x0.5° surface radiation grids within each 1°x1° region. The surface albedo is assumed to be 0.05 in computing the net surface SW flux, whereas the surface emissivity is assumed to be 0.97 in computing the net surface LW flux.

The first few months of the year 1998 are in the later phase of the 1997-1998 El Nino. Clouds in the strong convective Maritime continents are much reduced compared to the first few months of the year 1999. Figure 6 shows that the fractional cover (or amount) of high-level clouds of February 1998 and 1999 in the TWP. (It is noted that there are many GMS images missing in January 1998, and the results for this month are not shown.) A 5-km GMS pixel is identified as filled with high-level clouds if the GMS-measured T_b is <255 K. Also shown in the figure are the differences in cloud amounts and T_s between the two months. The high-level cloud amount in the neighborhood of the

maritime continents and SCS is smaller in February 1998 as compared to February 1999. The equatorial high-level cloud amount east of the dateline increases in February 1998 as compared to February 1999, indicating an eastward shift of convection center to the central equatorial Pacific. Correspondingly, the surface net downward radiation (SW+LW) increases significantly during the El Nino (February 1998) in the neighborhood of maritime continents and south of the Equator (Figure 7), where the intertropical convergence zone (ITCZ) is located during the Southern Hemispheric summer. Regions of enhanced heating with a magnitude >30 W m^{-2} is wide spread. The net surface heating in the equatorial region east of the dateline decreases by > 60 W m^{-2}, in accordance with the eastward shift of the convection center. These changes are expected to have a large impact on the distribution of sea surface temperature and the oceanic and atmospheric circulation.

Figure 8 shows the monthly variation of the sea surface radiation averaged over the TWP (30°S-30°N, 90°E-170°W). It can be seen in the upper panel that the SW heating in the first three months of 1998 is significantly larger than that of 1999 due to a less cloudy situation during El Nino. Averaged over the three months (January, February, and March), the SW heating of the ocean is 162.3 W m^{-2} for 1998 and 152.9 W m^{-2} for 1999. The change is large considering the facts that it is averaged over a season and over both ascending and descending regimes of the Hadley and Walker circulations. The minimum heating in June (Months 6 and 18) and December (Month 12) and the maximum heating in March and September are due to the seasonal shift of cloud bands with the solar position. In June (December), solar insolation at the top of the atmosphere is the largest in the Northern (Southern) Hemisphere where the ITCZ is located, resulting in the largest reflection of the solar radiation. Whereas in March and September, The latitudinal distribution of the insolation is much more uniform, and the domain-averaged insolation is larger when compared to June and December.

The middle panel of Figure 8 shows that the monthly variation of LW cooling of the TWP ocean is small, except for the first three months of 1998 when convection in the TWP is mostly suppressed, as shown in Figure 6. The lower panel of the figure shows that the net surface radiation (SW+LW) follows the SW radiation with a distinct seasonal variation.

The South China Sea summer monsoon system is an important component of the East and Southeast Asian climate. Improving the understanding of physical processes and evolution of the monsoon system are among the objectives of the SCSMEX conducted in May and June of 1998. The cloud systems associated with the onset, transition, and break stages of the monsoon directly affect the surface radiative heating, which in turn feedback to affect the dynamics of the monsoon. Figures 9 shows that the surface radiative heating of the South China Sea in May 1998 is smaller by 60 W m^{-2} than May 1999. The onset of the East Asian summer monsoon normally occurs in the month of May. The large change in the radiative heating as shown in the figure is expected to have a significant impact on the onset and evolution of the East Asian summer monsoon.

5. Atmospheric Solar Heating

It has long been an issue concerning whether clouds enhance the solar heating of the atmosphere [e.g. *Stephens and Tsay*, 1990]. *Cess et al.* [1995], *Pilewskie and Valero* [1995], and *Ramanathan et al.* [1995] studied this problem using different approaches and over different geographical regions and suggested that atmospheric solar heating increased significantly due to clouds and that the increase was approximately 25-30 Wm^{-2}. Subsequent studies [*Imre et al.*, 1996; *Li et al.*, 1997; Zender et al., 1997], also using various approaches, data sets, and geographical regions, gave mixed conclusions. On the other hand, there have been suggestions that the excess atmospheric heating due to clouds found in some studies is caused by the errors in estimating clear-sky surface SW flux [*Barker and Li*, 1995; *Li et al.*, 1997; *Arking*, 1999], which is necessary information for estimating the effect of clouds on atmospheric heating. This issue raises a very important question on the reliability of radiative transfer calculations, which is bound to have a critical impact on remote sensing and climate studies.

Solar heating of the atmosphere, Q, can be expressed as

$$Q_{clr} = S_{t,clr} - S_{s,clr} \qquad \text{for clear-sky} \qquad (4)$$

and

$$Q_{all} = S_{t,all} - S_{s,all} \qquad \text{for all-sky} \qquad (5)$$

where S is the net downward SW flux, the subscripts *t* and *s* denote the TOA and the surface, and *clr* and *all* denote the clear-sky and the all-sky, respectively. The effect of clouds on the atmospheric solar heating, or the atmospheric SW cloud radiative forcing (CRF), is then given by

$$\Delta Q = Q_{all} - Q_{clr} \tag{6}$$

Thus, evaluation of the effect of clouds on atmospheric solar heating involves four components of SW fluxes. Limited by the length of the CERES data currently available, our analysis of the atmospheric SW CRF is restricted to the 8-month period from January to August 1998.

5.1. Clear-Sky SW Radiation

The TOA clear-sky SW flux is available from the CERES ES-4 data archive. The surface clear-sky SW flux is not available from satellite measurements. Equation (1) is for surface SW flux in both cloudy and clear situations; clear-sky radiation and cloudy-sky radiation are not separately identified. Therefore, we rely on radiative transfer calculations for clear-sky surface SW flux. In studying the surface radiation during the TOGA COARE IOP and the SCSMEX IOP, *Chou and Zhao* [1997] and *Lin et al.* [2000] found that radiation model calculations of the clear-sky surface SW flux were in agreement with the radiometric measurements. During the eight months (January-August 1998) when TOA fluxes are available from CERES data archive, there are also aerosol optical thickness available over global oceans from the NASA Sea-viewing Wide Field-of-view Sensor (SeaWiFS) project. We assume that the aerosols are maritime sulfuric particles with little absorption of SW radiation. For the maritime aerosols, the single-scattering albedo is set to 0.996 and the asymmetry factor is set to 0.786. Using these aerosol parameters, together with the column water vapor amount retrieved from SSMI radiance measurements [*Wentz*, 1994], the SW fluxes at the TOA and the surface are computed using the radiation model of *Chou and Suarez* [1999]. The TOA and the surface SW fluxes are not sensitive to column ozone amount. A constant ozone amount, 0.320 $(\text{cm-atm})_{stp}$, typical of a midlatitude summer atmosphere is used in the calculations. The sea-surface albedo is fixed at 0.05.

Monthly variations of the clear-sky net downward SW flux at the TOA, $S_{t,clr}$, averaged over the TWP are shown by Curve A of Figure 10 taken from CERES data archive and Curve B taken from radiative transfer calculations. The two curves differ by 3-5 W m^{-2}, which is equivalent to a clear-sky albedo of 0.01. (The mean insolation at the TOA in the TWP is ~400 W m^{-2}.) The clear-sky net downward SW flux at the surface, $S_{s,clr}$, from radiative transfer calculations is shown by Curve D of Figure 10, and the clear-sky solar heating of the atmosphere, Q_{clr}, is shown in Figure 11 (Curves B and C). Curve B of Figure 11 is derived using $S_{t,clr}$ from CERES, and Curve C is derived using $S_{t,clr}$ from radiative transfer calculations. The clear-sky atmospheric SW heating changes very little from month to month. Averaged over the first eight months of 1998, Q_{clr} is 82 W m^{-2} if $S_{t,clr}$ is taken from CERES and is 78 W m^{-2} if $S_{t,clr}$ is taken from radiation model calculations.

5.2. All-Sky SW Radiation

The all-sky net downward SW flux at TOA, $S_{t,all}$, is taken from the CERES archive, and the all-sky net downward SW flux at the surface, $S_{s,all}$, is derived from Equation (1). The CERES E-4 data have a temporal resolution of 1 month and a spatial resolution of 2.5°x2.5° latitude-longitude. In Figure 10, Curve C shows the monthly-mean values of $S_{t,all}$ taken from CERES, and Curve E shows the monthly-mean values $S_{s,all}$ retrieved from GMS-measured albedo. The all-sky atmospheric SW heating, Q_{all}, is shown by Curve A of Figure 11. Following the all-sky net downward SW flux at the TOA, $S_{t,all}$ (Curve C, Figure 10), Q_{all} varies significantly from 93 W m^{-2} in June 1998 to 107 W m^{-2} in February and March 1998. Averaged over the eight months and the TWP, the value of Q_{all} is 100.2 W m^{-2}.

5.3. Cloud Radiative Forcing

The atmospheric solar heating, Q, in the TWP and the SCS , as well as the equatorial western Pacific (EWP), are given in Table 1. Numbers are mean values for the first eight months of 1998. The magnitudes of Q vary only slightly among the three domains. It is ~100 W m^{-2} for the all-sky solar heating and ~80 W m^{-2} for the clear-sky solar heating. Thus, clouds enhance the atmospheric solar heating by ~20 W m^{-2}. This number can be compared with the atmospheric CRF of +9 W m^{-2} estimated by *Chou et*

al. [1998] for the Pacific warm pool during the TOGA COARE IOP. *Chou et al.* [1998] used the ERBE TOA SW fluxes in November 1997-February 1998 as surrogate for the TOA SW fluxes in the TOGA COARE IOP (November 1992-February 1993), which could be the reason for the smaller atmospheric CRF estimated for the Pacific warm pool. This number can also be compared with the atmospheric CRF of +34 W m^{-2} estimated by *Ramanathan et al.* [1998].

A convenient parameter for measuring the atmospheric CRF is the ratio of the CRF at the TOA to that at the surface [e.g. *Cess et al.*, 1995],

$$R = (S_{t,all} - S_{t,clr}) / (S_{s,all} - S_{s,clr}) \quad (7)$$

Clouds do not have any effect on the atmospheric solar heating if R=0 and enhance the atmospheric solar heating if R>0. Table 1 shows that this parameter is ~1.6 for the three regions in the GMS domain. The TWP includes both ascending and descending regimes of the tropical circulation, whereas the EWP is mostly in the ascending regime with active convection. On the other hand, the SCS is under the strong influence of East Asian summer monsoon. Theoretical radiative transfer studies [e.g. *Chou et al.*, 1995] show that the value of R should depend on the cloud height and the solar zenith angle. The near-constant value of R in the tropical region indicates that the effects of those parameters are largely averaged out over large areas and long period of time. The clear-sky SW fluxes at the TOA given in Table 1 are model calculations. When the CERES clear-sky fluxes are used, the value of R reduces from ~1.6 to ~1.4.

It should be noted that the good agreement between the CERES-retrieved and model-computed clear-sky SW fluxes at the TOA does not necessarily imply that the model calculations of surface SW flux are accurate. Enhanced absorption by gases and particles in the atmosphere has little effect on the SW flux at the TOA but could have a large effect at the surface. Sample calculations show that, for a typical midlatitude summer atmosphere and a solar zenith angle of 60°, the net downward SW flux increases by ~2 W m^{-2} at the TOA but decreases by ~20 W m^{-2} at the surface when the water vapor amount (or the absorption coefficient) is doubled. The accuracy of the clear-sky surface SW flux, either from model calculations or from radiometric measurements, is difficult to assess.

Since the all-sky SW fluxes given in Table 1 are satellite retrievals, radiative transfer calculations of fluxes in cloudy atmospheres are not an issue here. However, the all-sky SW flux at the surface is empirically derived from the GMS-5 albedo measurement and validated against surface measurements. Its accuracy is constrained by the accuracy of the surface radiometric flux measurements. The atmospheric CRF is estimated from the flux components, S_t and S_s, averaged over long-period of time and large expanse of area. The spatial inhomogeneity of clouds and the inconsistency between the flux measurements from above and below clouds (cf. *Arking et al.*, 1996) are also not an issue here.

The CRF of 20 W m^{-2} shown in Table 1 is the flux convergence in the atmosphere, which involves four large components. Errors in each component can easily alter the estimate of the atmospheric CRF. Nevertheless, the numbers given in Table 1 represent our best estimate of the atmospheric CRF in the TWP and the SCS.

6. Summary

The surface SW radiation is known to correlate closely with the radiation at the top of the atmosphere. Using the empirical algorithms of *Chou and Zhao* [1997], the surface SW flux is derived as a function of the albedo in the visible spectral region measured by GMS-5 and the solar zenith angle. On the other hand, the surface LW radiation is tightly related to the temperature and humidity of the atmospheric boundary layer. It is derived as a function of the column water vapor amount, the sea surface temperature, and the brightness temperature in the infrared window region measured by GMS-5. The hourly surface radiation is derived for 0.5°x0.5° latitude-longitude regions. It is subsequently degraded to a temporal resolution of 1 day for 0.5°x0.5° latitude-longitude. The data set covers the GMS domain of 90°E-170°W and 40°S-40°N. Currently it has a length of 20 months from January 1998 to August 1999. This data set is useful for atmospheric and oceanic studies in the tropical western Pacific. It can also be used for intercomparison with other surface radiation data sets.

The satellite-derived surface SW and LW fluxes are validated with the surface radiometric measurements at the ARM Atmospheric Radiation and Cloud Station (ARCS) site located on Manus island (2.06°S, 147.43°E) in the TWP warm pool and the Dungsha island (20.70°N, 116.72°E) in the SCS. The validation uses surface radiation

measured in 15 months (January 1998-March 1999) at the ARCS site and in two months (May and June 1998) at the Dungsha site during the SCSMEX Intensive Observing Period. For the SW radiation, the bias between the surface measurements and the satellite retrieval is 7 W m^{-2} and the rms difference is 30 W m^{-2}. For the LW radiation, the bias is negligible, <1 W m^{-2}, and the rms difference is <7 W m^{-2}.

The surface radiation data set is used to study the effect of El Nino and the East Asian summer monsoon on the heating of the ocean. The first few months of 1998 were in the later phase of the 1997-1998 El Nino. The convection center in the maritime continents shifted eastward by ~40-50 degrees longitude to the east of the dateline. Compared to the first three months of 1999, the net radiative heating of the ocean in the maritime continent region increased by >40 W m^{-2} during the first three months of 1998. In contrast, the net radiative heating of the ocean in the central equatorial region decreased by >60 W m^{-2}. Averaged over the TWP, the net radiative heating of the ocean decreased by 10 W m^{-2} in the first three months of 1998 when compared to the first three months of 1999. In the South China Sea, the interannual variation of the net surface radiative heating in May and June 1998 is >60 W m^{-2}. These changes in long-term and large-area surface heating are expected to have a significant impact on oceanic and atmospheric circulations.

The surface radiation data set is also used to study the atmospheric cloud radiative forcing (CRF). To estimate the atmospheric CRF, it requires information on the clear- and all-sky net downward SW fluxes at the TOA and the surface. The all-sky net downward SW flux at the TOA is taken from the CERES data archive, which covers a period of eight months from January to August 1998. The clear-sky SW flux at the surface is computed using a radiative transfer model. The clear-sky SW flux at the TOA is either taken from the CERES data archive or from radiative transfer calculations. Averaged over the 8-month period, clouds enhance the atmospheric solar heating by 20 W m^{-2}, and the ratio of the CRF at the TOA to that at the surface is 1.4-1.6. Since estimation of the atmospheric CRF involves four flux components with a large magnitude, any errors in these fluxes can alter significantly the conclusion on the atmospheric CRF. Therefore, it is very important to establish accurate radiometric

measurements for validating model calculations of clear-sky radiation and satellite retrievals of all-sky radiation at the surface.

Acknowledgments. This study was supported by the Radiation Research Program, NASA Office of Earth Science. The NCEP sea surface temperature were provided by R. W. Reynolds. The GMS raw data were compiled by P. Flament and R. Bernstein, University of Hawaii. Si-Chee Tsay of NASA Goddarad Space flight Center provided the surface radiation data measured at the Dungsha island. The SSM/I-retrieved total precipitable water were produced by Remote Sensing Systems sponsored, in part, by NASA and NOAA (Principal Investigator; Frank Wentz). The Manus radiation data were obtained form the Atmospheric Radiation Measuring (ARM) Program sponsored by the U.S. Department of Energy. The CERES data were obtained from the NASA Langley Research Center EOSDIS Distributed Active Archive Center. The aerosol data are produced and distributed, respectively, by the SeaWiFS Project and the Distributed Active Archive Center at the NASA Goddarad Space Flight.

REFERENCES

Arking, A., M.-D. Chou and W. L. Ridgway, On estimating the effects of clouds on atmospheric absorption based on flux observations above and below cloud level. *Geophy. Res. Lett.*, *23*, 829-832, 1996.

Arking, A., The influence of clouds and water vapor on atmospheric absorption, *Geophys. Res. Lett.*, *26*, 2729-2732, 1999.

Barker, H. W., and Z. Li, Improved simulation of clear-sky shortwave radiative transfer in the CCC-GCM. *J Climate, 8*, 2213-2223, 1995

Cess, R. D., M. H. Zhang, P. Minnis, L. Corsetti, E. G. Dutton, B. W. Forgan, D. P. Garber, W. L. Gates, J. J. Hack, E. F. Harrison, X. Jing, J. T. Kiehl, C. N. Long, J.-J. Morcrette, G. L. Potter, V. Ramanathan, B. Subasilar, C. H. Whitlock, D. F. Young and Y. Zhou, Absorption of solar radiation by clouds: Observations versus models. *Science*, *267*, 496-499, 1995.

Chou, M.-D., Radiation budgets in the western tropical Pacific. *J Climate*, *7*, 1958-1971, 1994.

Chou, M.-D., A. Arking, J. Otterman and W. L. Ridgway, The effect of clouds on atmospheric absorption of solar radiation. *Geophy. Res. Lett.*, *22*, 1885-1888, 1995.

Chou, M. D., W. Zhao, Estimation and model validation of surface shortwave radiation and cloud radiative forcing using TOGA COARE measurements. *J. Climate*, *10*, 611-620, 1997.

Chou, M.-D., W. Zhao and S.-H. Chou, Radiation budgets and cloud radiative forcing in the Pacific warm pool during TOGA COARE. *J. Geophys. Res., 103*, 16967-16977, 1998.

Chou, M. D. and M. J. Suraez, A shortwave radiation Parameterization for atmospheric studies. *Volume 15, Technical Report Series on Global Modeling and Data Assimilation*. NASA/TM-1999-104606. pp40, 1999.

Chou, S.-H., W. Zhao, and M.-D. Chou, Surface Heat Budgets and Sea Surface Temperature in the Pacific Warm Pool During TOGA COARE, *J. Climate*, *13*, 634-649, 2000.

Gilgen, H., and A. Ohmura, The Global Energy Balance Archive. *Bull. Amer. Meteorol. Soc.*, *80*, 831-850, 1999.

Gupta, S. K., N. A. Ritchey, A. C. Wilber, C. H. Whitlock, G. G. Gibson, and P. W. Stackhouse Jr., A climatology of surface radiation budget derived from satellite data. *J. Climate*, *12*, 2691-2710, 1999.

Imre, D. G., E. H. Abramson, and P. H. Daum, Quantifying cloud-induced shortwave absorption: An examination of uncertainties and of recent arguments for large excess absorption, *J. Appl. Meteorol.*, *35*, 1991-2010, 1996.

Lau, K. M. Y. Ding, J. T. Wang, R. Johnson, T. Keenan, R. Cifelli, J. Gerlach, O. Thiele, T. Rickenbach, S. C. Tsay and P. H. Lin, A report of the field operations and early results of the South China Sea Monsoon Experiment (SCSMEX). *Bull. Amer. Meteor. Soc.*, in press.

Li, Z., and H. G. Leighton, Global climatologies of solar radiation budgets at the surface and in the atmosphere from 5 years of ERBE data. *J. Geophy. Res.*, *98*, 4919-4930, 1993.

Li, Z., L. Moreau, and A. Arking, On solar energy disposition: A perspective from observation and modeling. *Bull. Amer. Met. Soc.*, *78*, 1-18, 1997.

Mather, J. H., T. P. Ackerman, W. E. Clements, F. J. Barnes, M. D. Ivey, L. D. Hatfield, and R. M. Reynolds, An atmospheric radiation and cloud station in the tropical western Pacific, *Bull. Amer. Met. Soc.*, *79*, 627-642, 1998.

Pilewskie P., F. P. J. Valero, Direct observations of excess solar absorption by clouds, *Science*, *267*, 1626-1629, 1995.

Pinker, R. T., R. Frouin and Z. Li, A review of satellite methods to derive surface shortwave radiative fluxes. *Rem. Sen. Environ.*, *51*, 108-124, 1995.

Ramanathan, V., B. Subasilar, G. J. Zhang, W. Conant, R. D. Cess, J. T. Kiehl, H. Grassl, and L. Shi, Warm pool heat budget and shortwave cloud forcing: A missing physics? *Science*, *267*, 499-503, 1995.

Reynolds, R. W. and T. M. Smith, Improved global sea surface temperature analyses. *J. Climate, 7,* 929-948, 1994.

Rossow, W. B., and R. A. Schiffer, ISCCP Cloud data products. *Bull. Amer. Met. Soc.*, *72*, 2-20, 1991.

Wentz, F. J., *User's Manual SSM/I -2 Geophysical Tapes.* Tech. Rep. 070194, 20 pp., 1994. [Available from Remote Sensing Systems, Santa Rosa, CA.]

Wielicki, B. A., B. R. Barkstrom, E. F. Harrison, R. B. Lee III, G. L. Smith, and J. E. Cooper, Clouds and the Earth's Radiant Energy System (CERES): An earth observing system experiment. *Bull. Amer. Meteor. Soc.*, *77*, 853-868, 1996.

Stephens, G. L., and S.-C. Tsay, On the cloud absorption anomaly. *Q. J. R. Meteorol. Soc.*, *116*, 671-704, 1990.

Zender, C. S., B. B. Bush, S. K. Pope, A. Bucholtz, W. D. Collins, J. T. Kiehl, F. P. J. Valero and J. Vitko Jr, Atmospheric absorption during atmospheric radiation measurement (ARM) Enhanced Shortwave Experiment (ARESE). *J. Geophys. Res.*, *102*, 29901-29915, 1997.

Zhang, Y.-C., W. B. Rossow, and A. A. Lacis, Calculation of surface and top of atmosphere radiative fluxes from physical quantities based on ISCCP data sets. Part 1: Method and sensitivity to input data uncertainties. *J. Geophys. Res.*, *100*, 1149-1165, 1995.

Table 1. The All- and Clear-Sky Net Downward SW Fluxes at the TOA (S_t) and at the Sea Surface (S_s), and the Cloud Radiative Forcing (CRF) in the Tropical Western Pacific (30°S-30°N, 90°E-170°W), Equatorial Western Pacific (10°S-10°N, , 90°E-170°W), and the South China Sea (5°N-10°N, 105°W-115°W; 10°N-20°N, 110°W-120°W). Q is the Atmospheric Solar Heating. The Units are W m^{-2} for Fluxes and Fraction for the Parameter R.

	All-Sky	Clear-Sky	CRF
		Tropical Western Pacific	
S_t	315.4	354.0*	-38.6
S_s	215.2	276.5	-61.3
Q	100.2	77.5	22.7
R	--	--	1.59
		Equatorial Western Pacific	
S_t	319.6	365.6*	-46.0
S_s	212.9	283.1	-70.2
Q	106.7	82.5	24.2
R	--	--	1.53
		South China Sea	
S_t	335.9	371.2*	-35.3
S_s	232.4	289.0	-56.6
Q	103.5	82.2	21.3
R	--	--	1.60

- To be consistent with the clear-sky surface SW flux, the clear-sky TOA flux is taken from model calculations.

FIGURE CAPTIONS

Figure 1. Daily variations of the surface downward SW flux, $S_s^{\downarrow}$, measured at the Manus island and retrieved from GMS-5 albedo measurements during January 1998-March 1999. Because of missing GMS data, neighboring points are not necessarily consecutive days.

Figure 2. The surface downward SW flux, $S_s^{\downarrow}$, measured at Manus island vs. that retrieved from GMS-5 albedo measurements. Each point represents daily values in the period January 1998-March 1999.

Figure 3. Daily variations of the surface downward LW flux, $F_s^{\downarrow}$, measured at Manus island and retrieved from GMS-5 brightness-temperature measurements. Because of missing GMS data, neighboring points are not necessarily consecutive days.

Figure 4. Daily variations of the surface downward SW flux, $S_s^{\downarrow}$, measured at Dungsha island and retrieved from GMS-5 albedo measurements during the SCSMEX IOP (May-June 1998). Because of missing GMS data, neighboring points are not necessarily consecutive days

Figure 5. The surface downward SW flux, $S_s^{\downarrow}$, measured at Dungsha island vs. that retrieved from GMS-5 albedo measurements. Each point represents daily values in the SCSMEX IOP (May-June 1998).

Figure 6. Left panels show the spatial distributions of the high-level fractional cloud cover in February 1998 and February 1999. Right panels show differences in cloud cover and the sea surface temperature between February 1998 and February 1999. High-level clouds are identified using a threshold of T_b=255K, where T_b is the GMS-measured brightness temperature in the 11-μm window channel.

Figure 7. Spatial distribution of the surface net downward radiative (SW+LW) flux in February 1998 (upper panel), February 1999 (middle panel), and the difference between the two months (lower panel). Units are W m^{-2}.

Figure 8. Monthly variation of the surface net downward SW, LW, and total radiation averaged over the tropical western Pacific (30°S-30°N, 90°E-170°W). Fluxes are retrieved from radiances measured by the GMS-5 satellite. The first month corresponds to January 1998. Units of flux are W m^{-2}.

Figure 9. Same as Figure 7, except for May 1998 and May 1999.

Figure 10. Monthly variation of the net downward SW fluxes averaged over the oceanic region of 30°S-30°N, 90°E-170°W. Curve A: CERES clear-sky flux at TOA. Curve B: Model-calculated clear-sky flux at TOA. Curve C: CERES all-sky flux at TOA. Curve D: Model-calculated clear-sky flux at the surface. Curve E: GMS-retrieved all-sky flux at the surface. The first month corresponds to January 1998.

Figure 11. Monthly variation of atmospheric solar heating over the oceanic region of 30°S-30°N, 90°E-170°W. Curve A: All-sky atmospheric solar heating; Curve B: Clear-sky atmospheric solar heating using CERES clear-sky TOA flux; Curve C: Clear-sky atmospheric solar heating using model-calculated clear-sky TOA flux. The first month corresponds to January 1998.

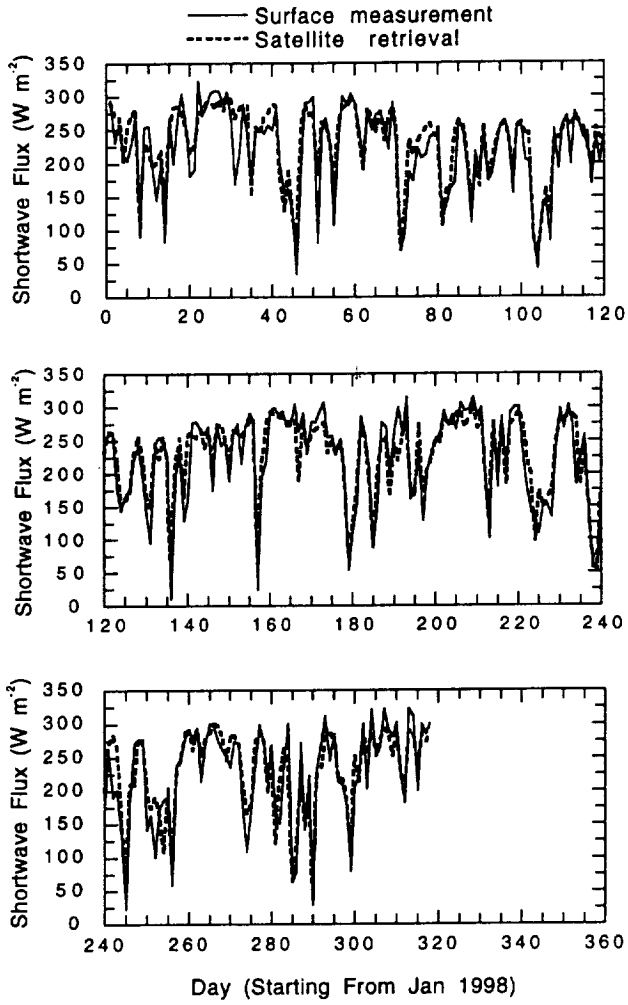
Surface measurement
Satellite retrieval
Shortwave Flux (W m-2)
0
50
100
150
200
250
300
350
0
20
40
60
80
100
120
120
140
160
180
200
220
240
240
260
280
300
320
340
360
Day (Starting From Jan 1998)

Figure 1

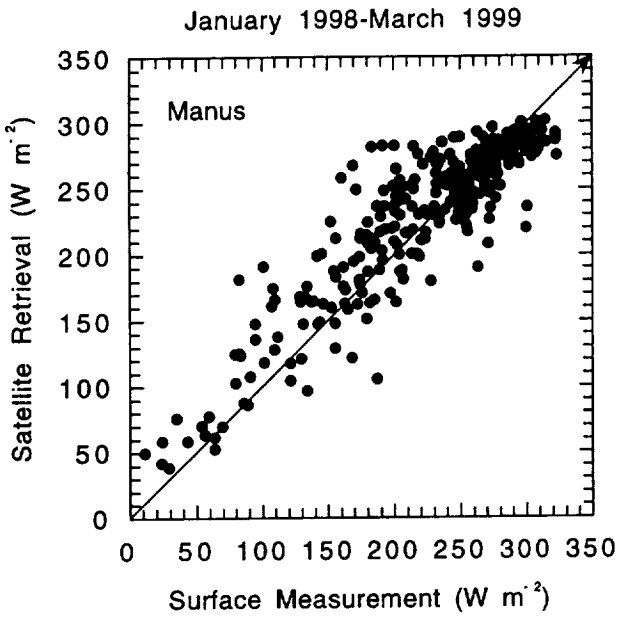
January 1998-March 1999
Manus
Satellite Retrieval (W m-2)
Surface Measurement (W m-2)
0
50
100
150
200
250
300
350

Figure 2

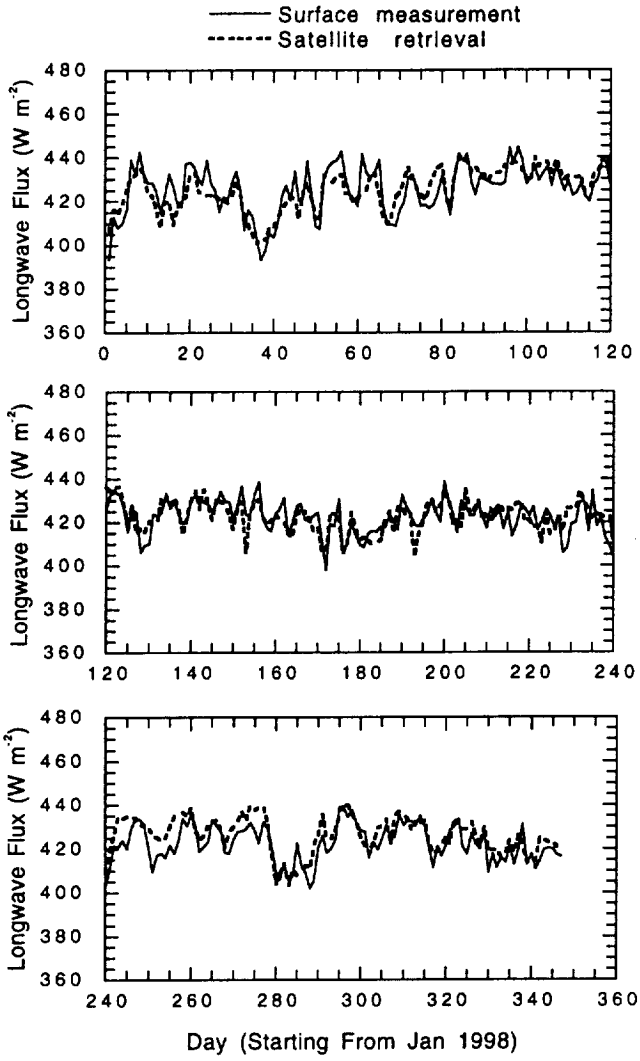
Surface measurement
Satellite retrieval
Longwave Flux (W m-2)
480
460
440
420
400
380
360
0
20
40
60
80
100
120
120
140
160
180
200
220
240
240
260
280
300
320
340
360
Day (Starting From Jan 1998)

Figure 3

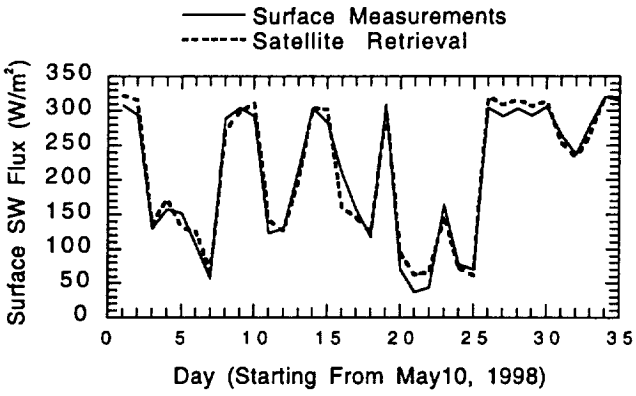
Surface Measurements
Satellite Retrieval
Surface SW Flux (W/m²)
350
300
250
200
150
100
50
0
0
5
10
15
20
25
30
35
Day (Starting From May10, 1998)

Figure 4

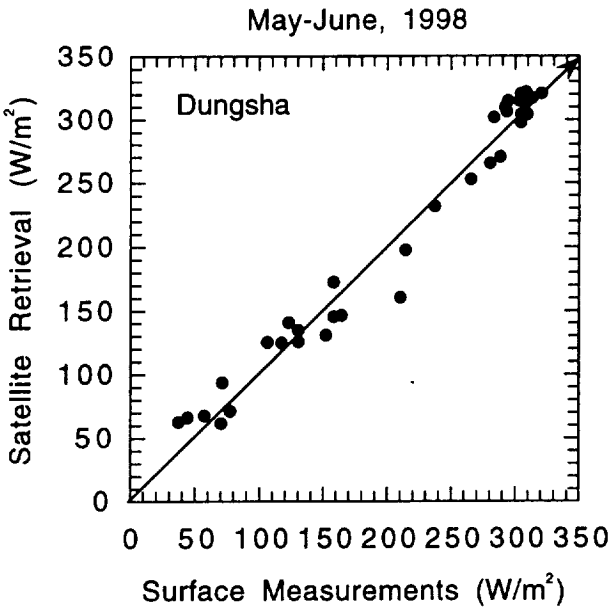
May-June, 1998
Dungsha
Satellite Retrieval (W/m²)
Surface Measurements (W/m²)
0
50
100
150
200
250
300
350

Figure 5

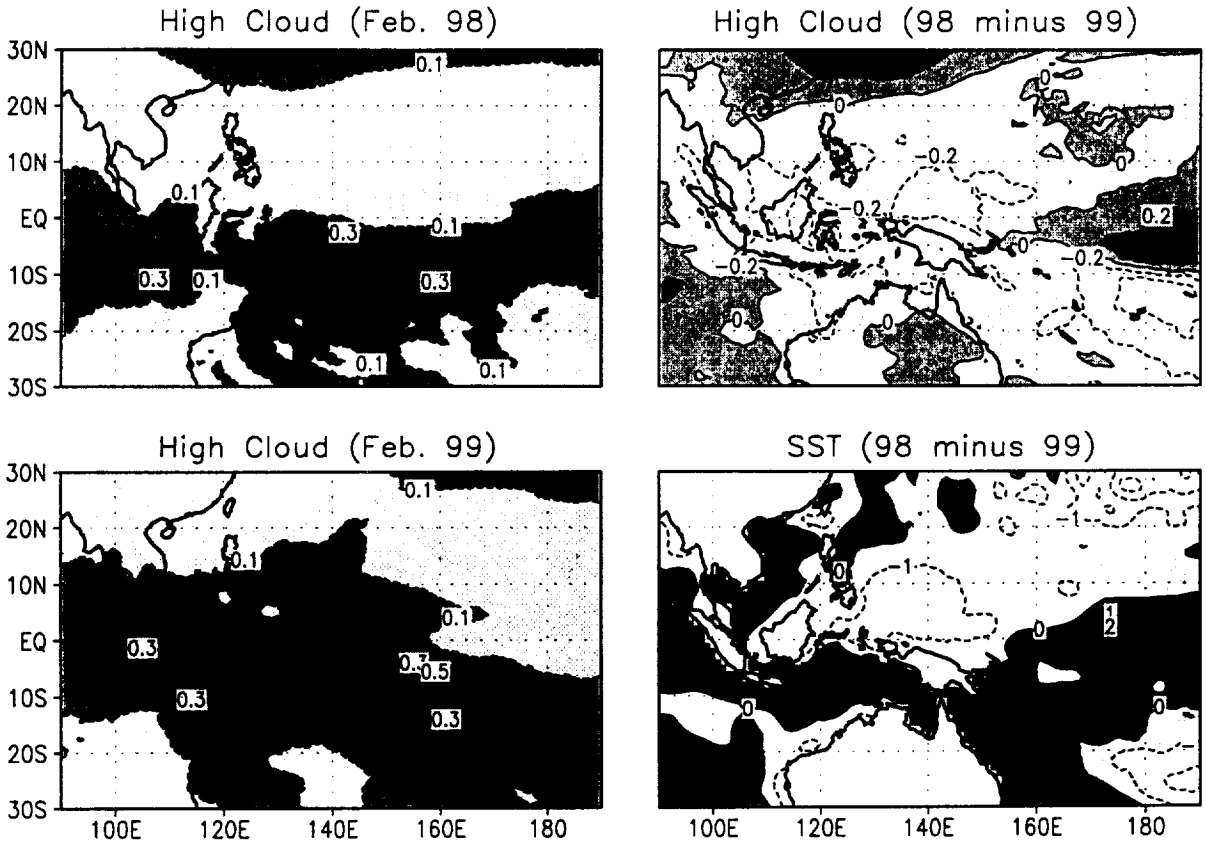
High Cloud (Feb. 98)
High Cloud (98 minus 99)
High Cloud (Feb. 99)
SST (98 minus 99)
30N
20N
10N
EQ
10S
20S
30S
100E
120E
140E
160E
180

Figure 6

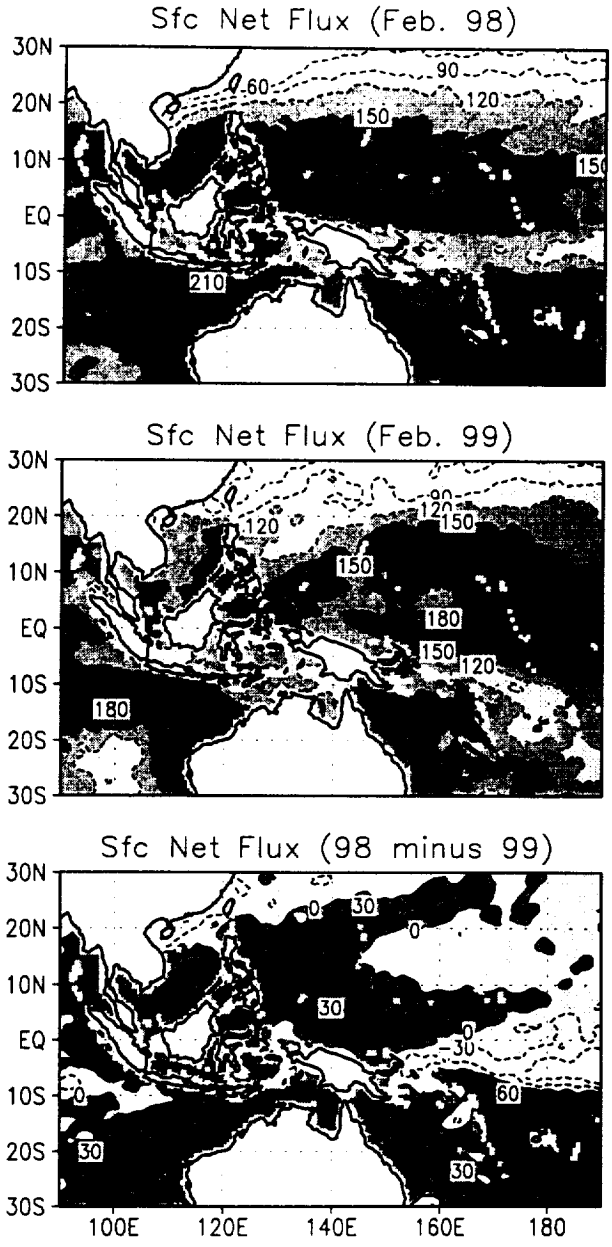
Sfc Net Flux (Feb. 98)
30N
20N
10N
EQ
10S
20S
30S
0
60
90
120
150
150
210
Sfc Net Flux (Feb. 99)
120
120
150
150
180
150
120
180
Sfc Net Flux (98 minus 99)
0
30
0
30
0
30
0
60
0
30
30
100E
120E
140E
160E
180

Figure 7

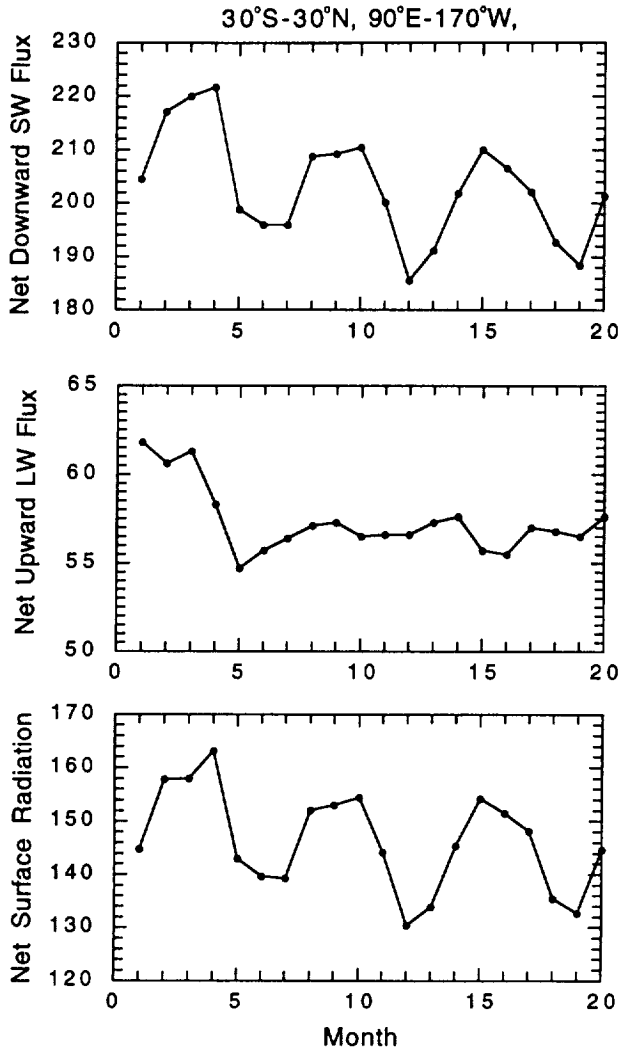
30°S-30°N, 90°E-170°W,
Net Downward SW Flux
230
220
210
200
190
180
0
5
10
15
20
Net Upward LW Flux
65
60
55
50
0
5
10
15
20
Net Surface Radiation
170
160
150
140
130
120
0
5
10
15
20
Month

Figure 8

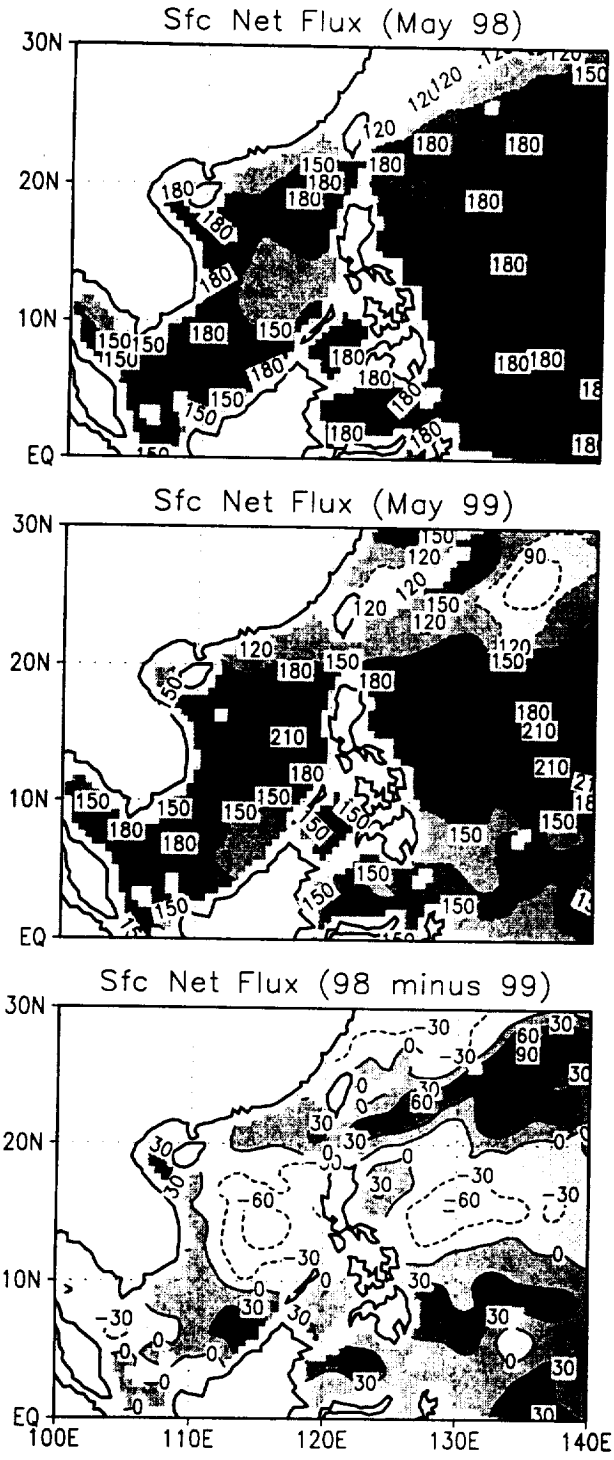
Sfc Net Flux (May 98)
Sfc Net Flux (May 99)
Sfc Net Flux (98 minus 99)
30N
20N
10N
EQ
100E
110E
120E
130E
140E

Figure 9

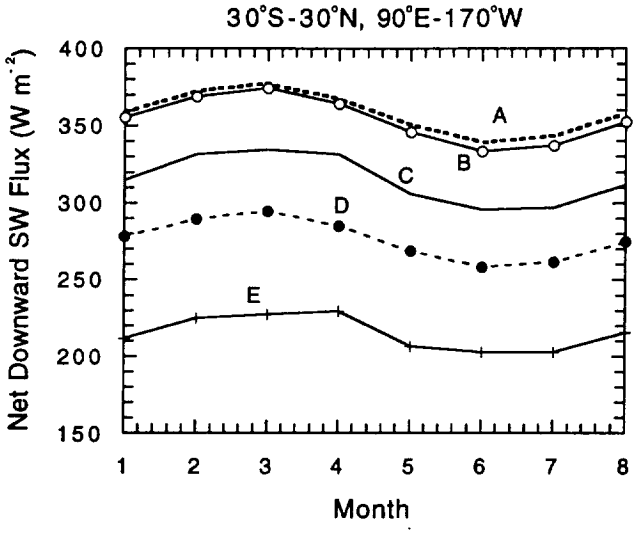
30°S-30°N, 90°E-170°W
Net Downward SW Flux (W m⁻²)
400
350
300
250
200
150
1
2
3
4
5
6
7
8
Month
A
B
C
D
E

Figure 10

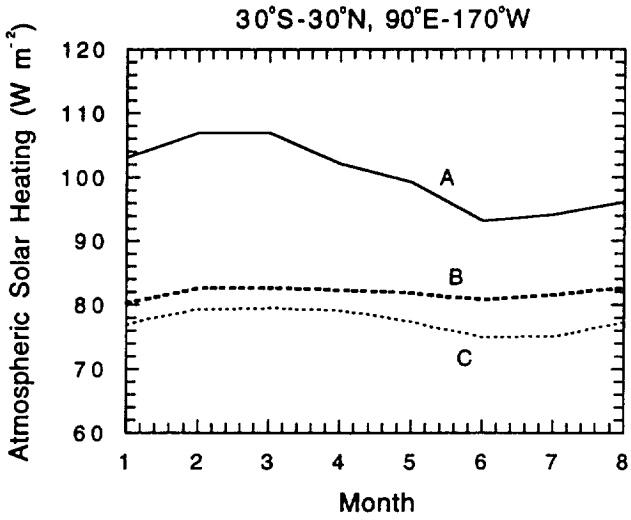
30°S-30°N, 90°E-170°W
Atmospheric Solar Heating (W m^{-2})
120
110
100
90
80
70
60
A
B
C
1
2
3
4
5
6
7
8
Month

Figure 11